Supporting Information

Silicon Diphosphide: A Si-Based Three-Dimensional Crystalline Framework as a High-Performance Li-Ion Battery Anode

Hyuk-Tae Kwon[a], *Churl-Kyoung Lee*[a], *Ki-Joon Jeon,*[*b] *and Cheol-Min Park*[* a]

[a]School of Materials Science and Engineering, Kumoh National Institute of Technology, 61 Daehak-ro, Gumi, Gyeongbuk 39177, Republic of Korea

[b]Department of Environmental Engineering, Inha University, 100 Inha-ro, Nam-gu, Incheon, 22212, Republic of Korea

[*] Corresponding authors.

[*]Ki-Joon Jeon. Tel.: +82-32-860-7509

E-mail: kjjeon@inha.ac.kr

[*]Cheol-Min Park. Tel.: +82-54-478-7746; Fax: +82-54-478-7769

E-mail: cmpark@kumoh.ac.kr

I. Preparation of the SiP_2

The SiP_2 was synthesized using a HEBM process for 20 h and it was analyzed using HRTEM to confirm its crystallinity, as shown in Figure S1. HRTEM images combined with SAED patterns confirmed well developed, crystalline micron-sized SiP_2 particles consisting of agglomerated ca. 20-30 nm sized nanocrystallites (Figure S1).

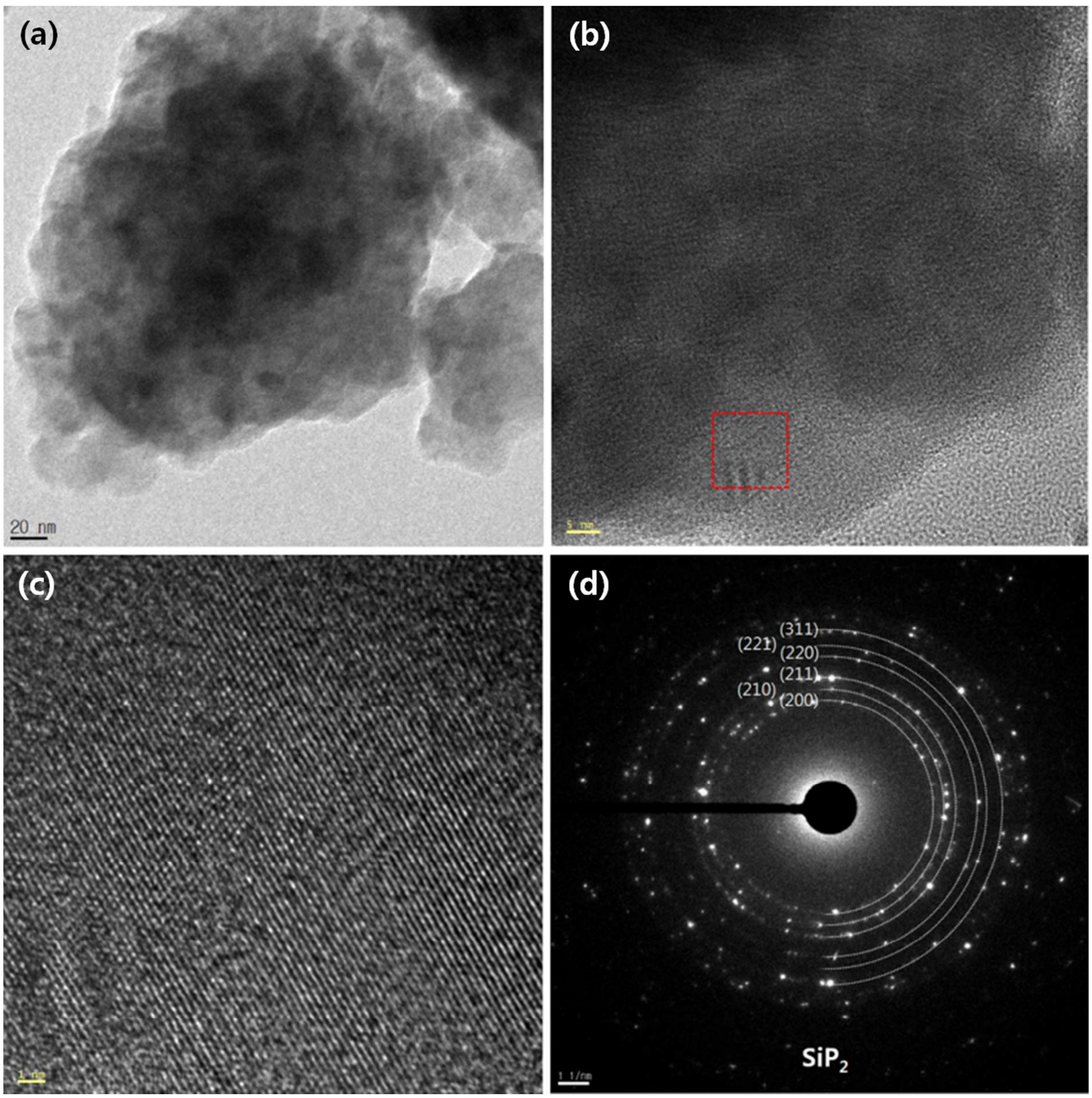

Figure S1. Morphological characteristics of the SiP_2. (a) TEM bright-field image. (b) HRTEM image. (c) HRTEM image corresponding to the selected regions in the HRTEM image. (d) SAED patterns of the selected regions in the HRTEM image.

II. Electrochemical performances of the Si and P electrodes

Figures S2(a) and S2(b) show the voltage profiles for the Si and black-P electrodes at a current density of 100 mA g^{-1}. The Si electrode showed very high discharge and charge capacities of 3645 and 2510 mAh g^{-1}, respectively, with a Coulombic efficiency of 68.9% [Fig. S2(a)]. Given the theoretical capacity of 3578 mAh g^{-1} (calculated based on the final phase of $Li_{15}Si_4$) of Si at room temperature, we could conclude that the Si was fully reacted with Li. However, the Si electrode exhibited poor capacity retention, corresponding to approximately 11.4% of the initial charge capacity after the 10th cycle. Figure S2(b) shows the voltage profile of the black P, which was synthesized using high-energy ball milling for 24 h. The black-P electrode also showed very high discharge and charge capacities of 2257 and 1280 mAh g^{-1}, respectively, with a Coulombic efficiency of 56.7%. Given the theoretical capacity of 2596 mAh g^{-1} (calculated based on the final phase of Li_3P) of P, the P was highly reacted with Li. However, the P electrode also exhibited poor capacity retention, corresponding to approximately 3.9% of the initial charge capacity after the 10th cycle.

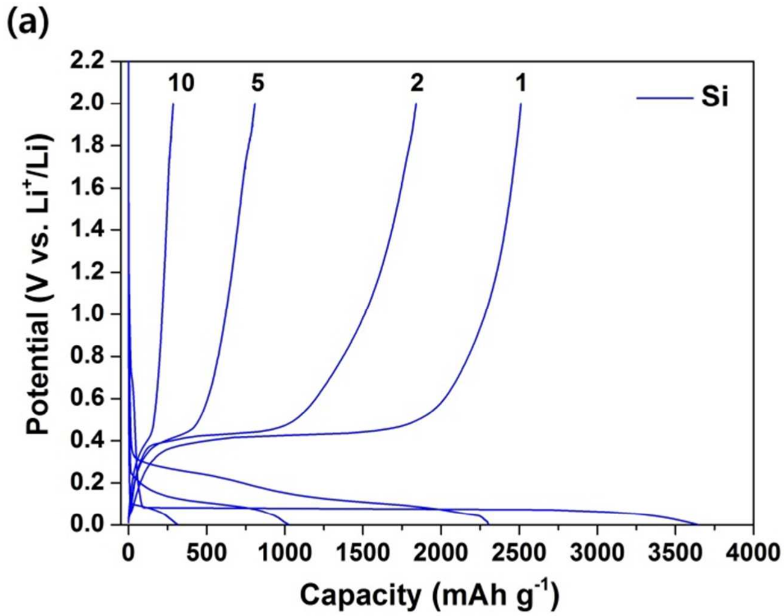

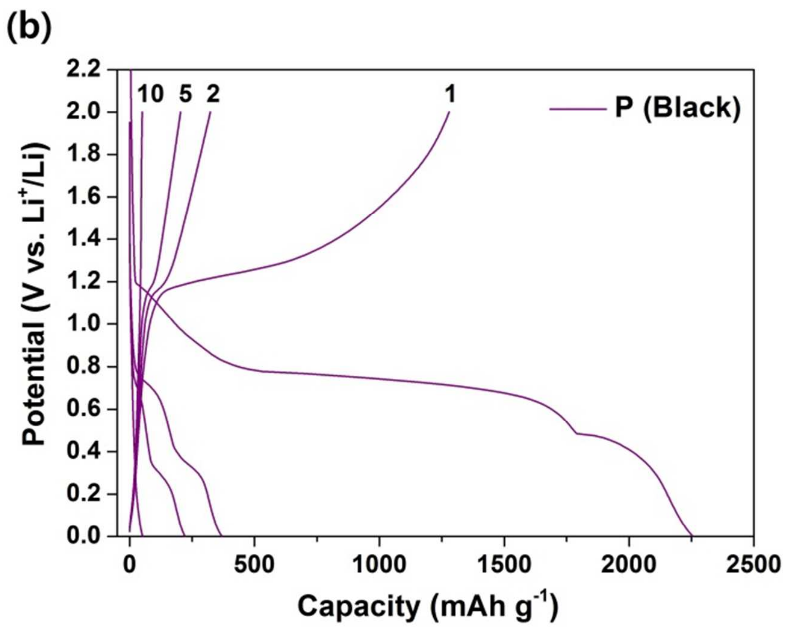

Figure S2. Electrochemical performances of the Si and black-P electrodes. (a) Voltage profiles of the Si electrode at a current density of 100 mA g^{-1}. (b) Voltage profiles of the black-P electrode at a current density of 100 mA g^{-1}.

III. ^{7}Li NMR spectra analysis of the SiP_2 electrode during initial cycling

For the solid-state NMR, all spectra were obtained using a 400 MHz solid-state NMR at KBSI Daegu center in Korea, operating at 79.488 MHz for ^{29}Si and 155.5 MHz for ^{7}Li. The lithiated- and delithiated-electrode samples of about 20 mg each were dried and transferred to 4 mm zirconia rotors in an Ar-filled glove box. The rotors were sealed with Kel-F caps that were airtight. All spectra were acquired under magic-angle-spinning (MAS) conditions with spin rates of 10 kHz for ^{29}Si and 12 kHz for ^{7}Li, using a single-pulse sequence. The pulse-repetition-delay times were 3 s for ^{29}Si and 5 s for ^{7}Li. All of the units in the chemical shifts are expressed in ppm and referenced relative to tetramethylsilane for ^{29}Si and to $LiAsF_6$ for ^{7}Li.

Solid-state ^{7}Li NMR was performed at the selected potentials indicated in the DCP [Fig. 2(a)], and the results are presented in Figure S3**.** When the potential was lowered from the open-circuit potential to 0.55 V, the ^{7}Li NMR results depicted two peaks comprised of a large peak at 3.3 ppm, corresponding to the Li_xSiP_2 ($x \leq 1.8$) phase, and a small Li-salt-in-electrolyte peak of -0.85 ppm (t_1 in Fig. S3)[1,2]. At a further discharged state of 0.25 V, the ^{7}Li NMR peak was slightly shifted to the left (6.7 ppm, t_2 in Fig. S3). When the potential was fully discharged at 0 V, the ^{7}Li NMR (t_3 in Fig. S3) spectrum definitely showed the formation of the $Li_{13}Si_4$ (11.5 ppm) and Li_3P (22.2 ppm) phases at room temperature[3], whereas when the SiP_2 electrode was in a fully charged state of 2 V, the ^{7}Li NMR peak was slightly shifted to the right (4.2 ppm, t_5 in Fig. S3), results that were caused by Li remaining after the charge reaction[4].

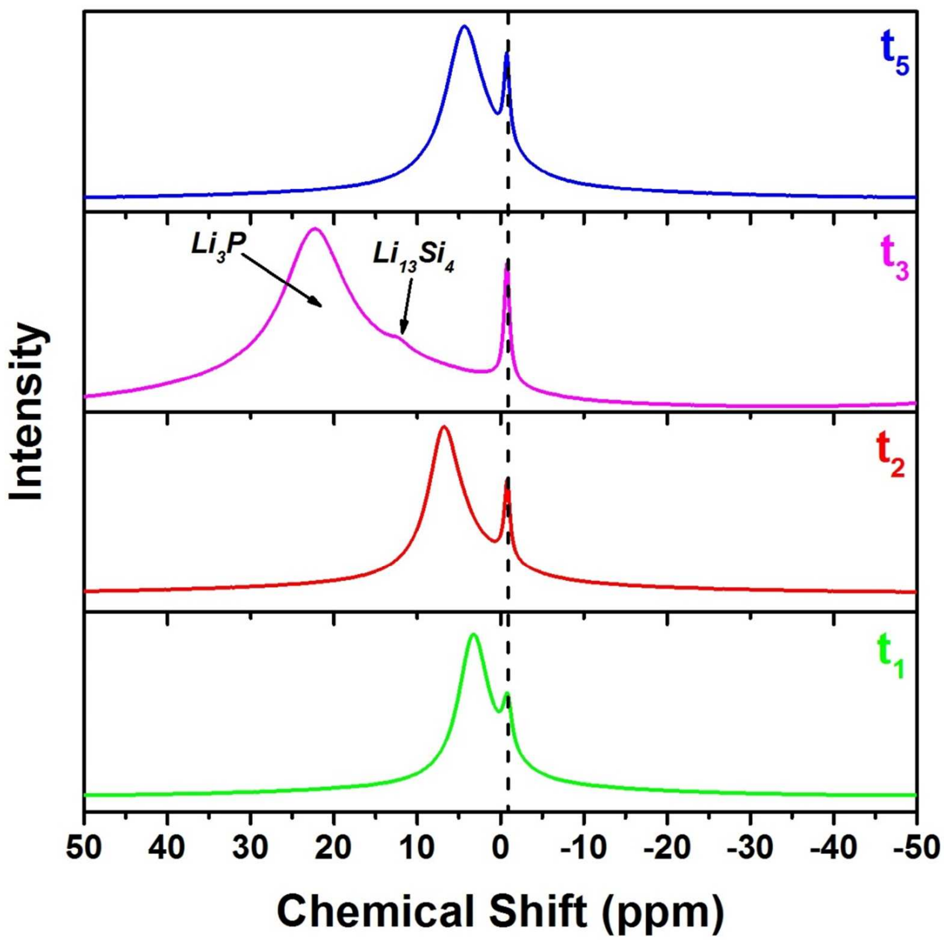

Figure S3. ^{7}Li NMR spectra analysis for the SiP_2 electrode at the selected potentials indicated in the DCP results.

IV. Preparation of the nanostructured SiP_2/C composite

The nanostructured SiP_2/C composite was prepared using an additional HEBM process for 6 h and was analyzed using XRD, as shown in Figure S4. The XRD pattern of the nanostructured SiP_2/C composite confirmed that no other crystalline phases were present.

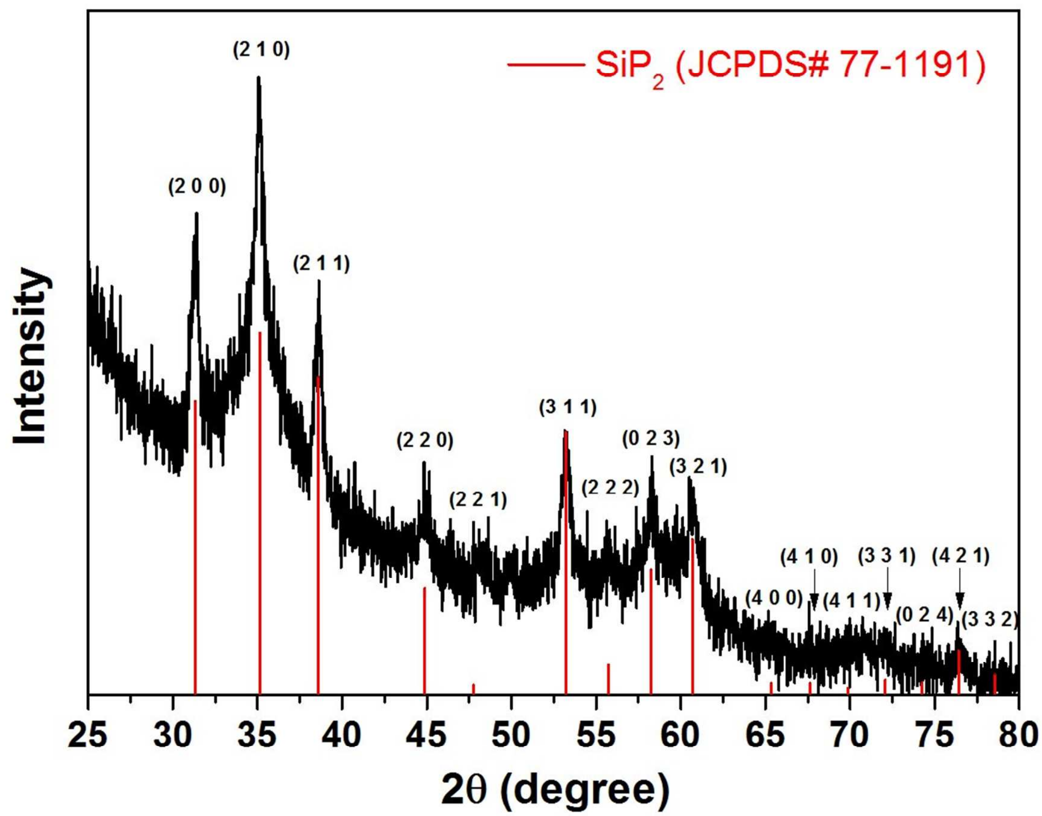

Figure S4. XRD analysis confirming the phases of the nanostructured SiP_2/C composite.

V. Electrochemical performance of the ball-milled carbon (Super P) electrode

Figure S5 shows the electrochemical performance of the ball-milled amorphous-carbon (Super P) electrode. Figure S5(a) shows the voltage profile of the ball-milled amorphous-carbon electrode at a current density of 100 mA g^{-1}. The ball-milled amorphous-carbon electrode showed high initial discharge and charge capacities of 916 and 560 mAh g^{-1}, respectively, with a Coulombic efficiency of 61.1%. The ball-milled amorphous-carbon electrode also showed a relatively stable capacity retention, corresponding to approximately 81.1% of the initial charge capacity after the 100th cycle (Fig. S5(b)).

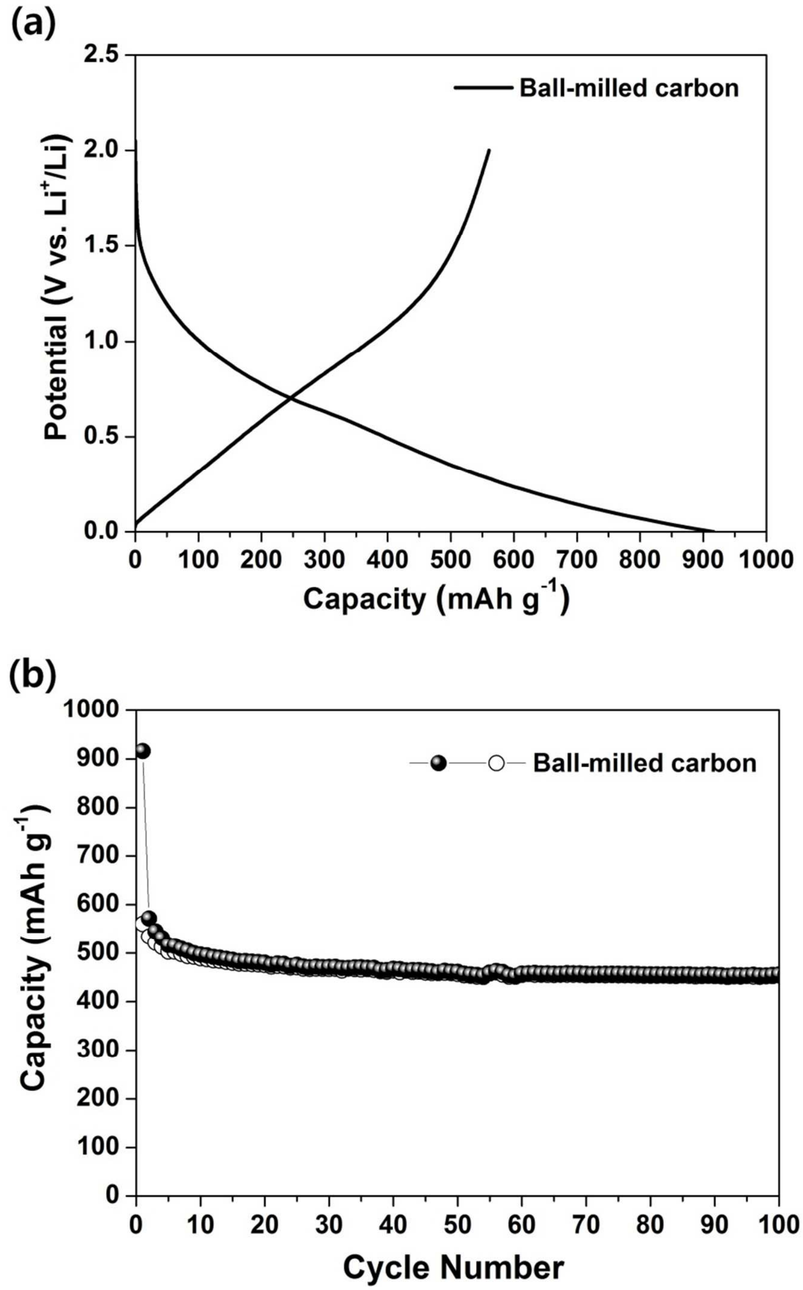

Figure S5. Electrochemical performances of the ball-milled amorphous-carbon (Super P) electrode. (a) Voltage profiles of the ball-milled amorphous-carbon electrode at a current density of 100 mA g^{-1}. (b) Cycle behavior of the ball-milled amorphous-carbon electrode.

VI. Differential capacity plot of the SiP_2/C nanocomposite electrode

Figure S6 shows the DCP result of SiP_2/C nanocomposite electrode was well coincided with that of SiP_2 electrode, which demonstrates that the SiP_2/C nanocomposite electrode also has the three-step electrochemical-reaction mechanism, sequentially comprised of a topotactic transition (0.55-2 V), an amorphization (0.25-2 V), and a conversion (0-2 V).

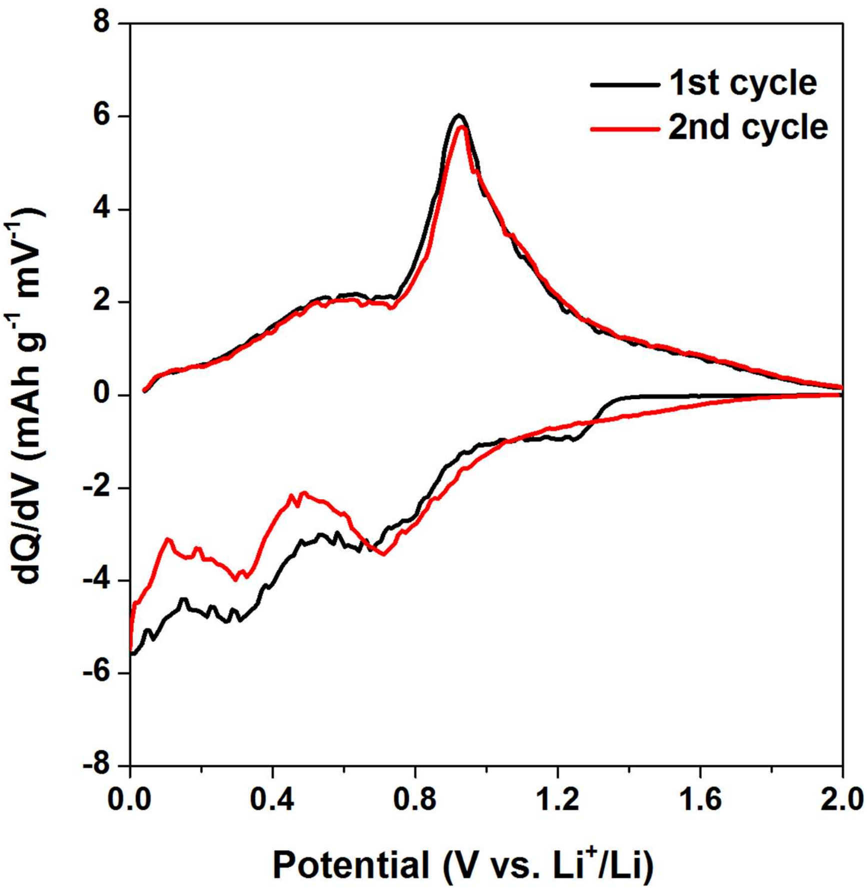

Figure S6. DCP result of SiP_2/C nanocomposite electrode for the first and second cycles.

VII. Rate-capability tests of the nanostructured SiP_2/C composite electrode

The rate-capability tests of the SiP_2/C nanocomposite electrode were also performed within the potential range of the amorphization (0.25-2 V) and topotactic-transition (0.55-2 V) steps. Figure S7 shows the voltage profiles of the SiP_2/C nanocomposite electrode as a function of the *C* rate, where *C* is defined as the full use of the restricted charge capacity of 1100 mAh g^{-1} (amorphization step) and 500 mAh g^{-1} (topotactic-transition step) in 1 h. In the case of the amorphization step [Fig. S7(a)], it had high charge capacities of 990 (1*C* rate) and 820 mAh g^{-1} (3*C* rate), respectively, corresponding to approximately 88% and 73% of the charge capacity at a rate of 0.1*C*. In the case of the potential range of the topotactic-transition step [Fig. S7(b)], it had charge capacities of 455 (1*C* rate) and 395 mAh g^{-1} (3*C* rate), corresponding to approximately 93% and 81%, respectively, of the charge capacity at a rate of 0.1*C* with stable cycling behavior.

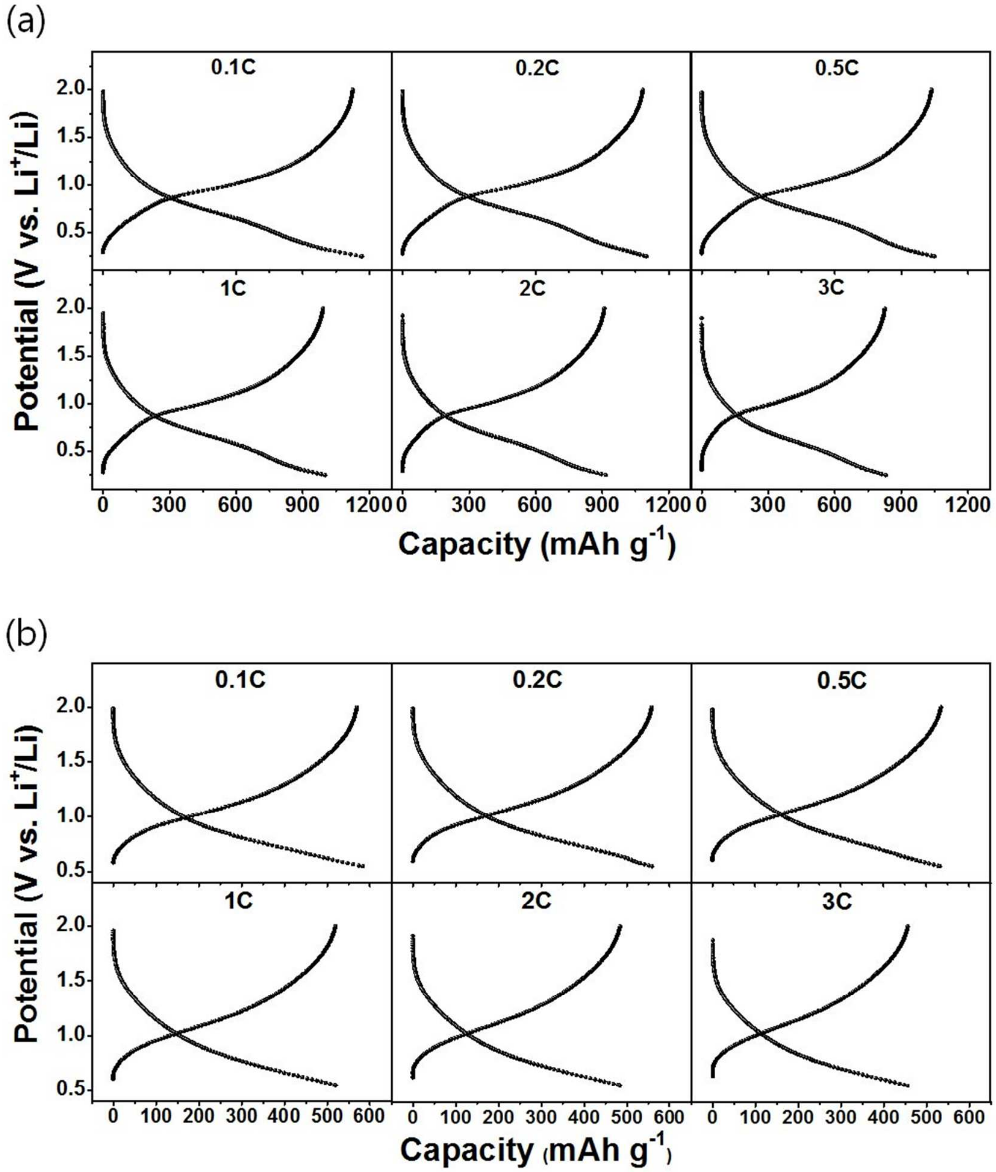

Figure S7. Rate-capability results of the nanostructured SiP_2/C composite electrode. (a) Voltage profiles at different current rates within the potential range of the amorphization step (0.25-2 V). (b) Voltage profiles at different current rates within the potential range of the topotactic-transition step (0.55-2 V).

References

[1] Goward, G. R.; Nazar, L. F.; Power, W. P. Electrochemical and Multinuclear Solid-State NMR Studies of Tin Composite Oxide Glasses as Anodes for Li Ion Batteries. *J. Mater. Chem.* **2000**, *10*, 1241-1249.

[2] Marino, C.; Boulet, L.; Gaveau, P.; Fraisse, B.; Monconduit, L. Nanoconfined Phosphorus in Mesoporous Carbon as An Electrode for Li-Ion Batteries: Performance and Mechanism. *J. Mater. Chem.* **2012**, *22*, 22713-22720.

[3] Key, B.; Bhattacharyya, R.; Morcrette, M.; Seznec, V.; Tarascon, J.-M.; Grey, C. P. Real-Time NMR Investigations of Structural Changes in Silicon Electrodes for Lithium-Ion Batteries. *J. Am. Chem. Soc.* **2009**, *131*, 9239-9249.

[4] Key, B.; Morcrette, M.; Tarascon, J.-M.; Grey, C. P. Pair Distribution Function Analysis and Solid State NMR Studies of Silicon Electrodes for Lithium Ion Batteries: Understanding the (De)Lithiation Mechanisms. *J. Am. Chem. Soc.* **2011**, *133*, 503-512.